Inorganica Chimica Acta 363 (2010) 2318–2324

Contents lists available at ScienceDirect

Inorganica Chimica Acta

journal homepage: www.elsevier.com/locate/ica

High-coordinated lanthanum(III) complexes with new mono- and bidentate phosphoryl donors; spectroscopic and structural aspects

Khodayar Gholivand *, Hamid Reza Mahzouni, Mehrdad Pourayoubi, Shadi Amiri

Department of Chemistry, Tarbiat Modares University, P.O. Box 14115-175, Tehran, Iran

ARTICLE INFO

Article history:
Received 7 December 2009
Received in revised form 20 March 2010
Accepted 24 March 2010
Available online 29 March 2010

Keywords:
Bidentate
Counter ion
Lanthanum(III) complex
Phosphoryl
X-ray crystallography
Hydrogen bonding

ABSTRACT

Monodentate and bidentate ligands PhNHP(O)(NC_4H_8O)$_2$ (**1**) and PhC(O)NHP(O)(NH(*tert*-C_4H_9))$_2$ (**2**) were used to prepare new 7, 9 and 10-coordinated lanthanum(III) complexes; La(**1**)$_2$$Cl_3$($H_2O$)$_2$ (**3**), La(**1**)$_2$(NO_3)$_3$$H_2O$.La(**1**)$_2$($NO_3$)$_3$$CH_3CN$ (**4**) and La(**2**)$_2$(NO_3)$_3$ (**5**), respectively. Crystallization of compound **2** in CH_3OH:CH_3CN leads to one conformer in contrast to the crystallization result from $CHCl_3$:*n*-C_7H_{16} (two conformers). Compound **4** contains two independent nine-coordinated La(III) complexes that are different in the solvated molecules (H_2O and CH_3CN). Some structural and electronic perturbations in coordinated ligand were occurred upon complexation, that are confirmed by increase of $^2J_{PH}$, $^3J_{PH}$ and $^6J_{PH}$ coupling constants from the free ligand **1** to complexes **3** and **4**. The steric repulsions in the first coordination sphere of La^{3+} ion, metal–ligand (M–L) binding strength and P=O stretching frequency are very influenced by changing the counter ion from Cl^- to NO_3^-. Comparing the X-ray crystallography data of free ligand **2** with bis-chelated complex **5**, it is found that the phosphoryl group is more reactive than carbonyl counterpart. A blue shift of the ν(N–H) vibration is observed in line with the weakening of the hydrogen bond from N–H···$O_{Phosphoryl}$ in **1** to N–H···Cl in **3**. Three dimensional butterfly-shape structures are seen in the unit cell of complex **3**, which are produced by O_{Water}–H···$O_{Morpholine}$ hydrogen bonds.

1. Introduction

Lately, a great intense of researches have been focused on the chemistry of phosphoryl–lanthanide complexes because of their importance in biological sciences [1–4], luminescent systems [5–8] and nuclear waste reprocessing [9,10]. The highly oxophilic nature of lanthanides makes they interact strongly with phosphoryl donors [11]. Up to now, various bidentate RC(O)CH_2P(O)(R′)$_2$ and monodentate (R)$_3$PO ligands have been extensively used to extract and separate of lanthanides and actinides [12–16]. Furthermore, some of the organophosphorus–lanthanide(III) [17–22] and complexes of Ce, Eu and Sm with RC(O)NHP(O)(NHR′)$_2$ ligands have been reported [23–25]. Also, the structural, electronic and energy features of lanthanides and actinides complexes of organophosphorus ligands have been theoretically investigated [26–32]. To our knowledge, there are a few reports (experimental or theoretical) of high coordinated La(III)-[P(O)(RC(O)NH)(NHR)$_2$] and La(III)-P(O)(NHR)(NHR′)$_2$ complexes. Using the quantum mechanical calculations we have already shown that cation affinity of phosphoramides is very close to that of organophosphorus ligands from the energy point of view. Taking into account that the synthesis pathway of phosphoramides is relatively inexpensive with respect to organophosphorus, they can be considered as efficient complexant agents for lanthanide [33]. Thus, in the present study, two new ligands, *N*-phenyl-*N*′,*N*″-bis(morpholinyl) phosphoric triamide (**1**) and *N*-benzoyl-*N*′,*N*″-bis(*tert*-butyl) phosphoric triamide (**2**) were used to prepare the 7-, 9- and 10-coordinated La(III) complexes **3–5** (Schemes 1 and 2). To achieve ligands with a good electron donating ability of phosphoryl group, we have selected both of aliphatic and aromatic substituents. To reach more hydrogen bonds in the solid state, the morpholine rings were selected as amine substituent in **1**. The electronic distribution and geometry of atoms in X–H···Y systems (X and Y are electronegative atoms) affect the strength of the hydrogen bond and also of the X–H bond [34,35]. Based on these theories, the hydrogen bonds in free ligands and complexes were compared. The phosphorus–hydrogen coupling constants, the stretching frequencies of the N–H, P=O and C=O bonds and the M–O, P=O and P–N bond lengths were compared to realize the structural reorganizations of the ligands upon complex formation.

2. Experimental

2.1. X-ray crystallography

Single crystals of compounds **3–5** obtained from a mixture of CH_3OH:CH_3CN (with ratio 1:4) at room temperature. X-ray data

* Corresponding author. Tel.: +98 21 82883443; fax: +98 21 8006544.
E-mail address: gholi_kh@modares.ac.ir (K. Gholivand).

0020-1693/$ - see front matter © 2010 Elsevier B.V. All rights reserved.
doi:10.1016/j.ica.2010.03.064

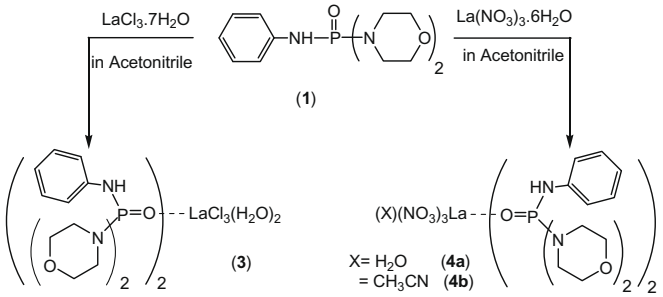

Scheme 1. Synthesis pathway of complexes **3** and **4** from the free ligand **1**.

of compounds **1** and **5** were collected on CAD4 Enraf-Nonius and for compounds **3** and **4** on a Bruker SMART APEX2 CCD area detector single crystal diffractometer with graphite monochromated Mo Kα radiation (λ = 0.71073 Å). The structures were refined with SHELXL-97 [36] by full matrix least squares on F^2. The crystallographic data and the details of the X-ray analysis of the compounds **1** and **3–5** are summarized in Table 1.

2.2. Instrumentation

^{1}H, ^{13}C and ^{31}P spectra were recorded on a Bruker Avance DRS 500 spectrometer. ^{1}H and ^{13}C chemical shifts were determined relative to internal TMS, ^{31}P chemical shifts relative to 85% H_3PO_4 as external standard. Infrared (IR) spectra were recorded on a Shimadzu model IR-60 spectrometer using KBr pellets. Elemental analysis was performed using a Heraeus CHN-O-RAPID apparatus.

2.3. Preparation of ligand P(O)(PhNH)(NC_4H_8O)$_2$; (*1*)

To a stirred solution of *N*-phenyl-phosphoramidic dichloride (1 mmol) in dry acetonitrile (35 ml), a solution of 4 mmol morpholine was added dropwise at −5 ℃. After 10 h stirring, the solvent was evaporated under vacuum and the white powder was washed with distilled water and recrystallized from a mixture of CH_3OH:$CHCl_3$ (1:3). Yield 75%, M.p. 181°C, *Anal.* Calc. for $C_{14}H_{22}N_3O_3P{\cdot}0.25CHCl_3$: C, 50.16; H, 6.57; N, 12.32. Found: C, 50.48; H, 6.65; N, 12.21%. ^{1}H NMR ($CDCl_3$, 500.13 MHz, 298 K): δ = 3.18 (m, 8H, CH_2), 3.60 (m, 8H, CH_2), 5.11 (d, $^2J_{PH}$ = 8.1 Hz, 1H, NH), 6.98 (t, $^3J_{HH}$ = 7.6 Hz, 1H, Ar–H), 7.08 (d, $^3J_{HH}$ = 7.6 Hz, 2H,

Scheme 2. Synthesis pathway of complex **5** from **2**.

Table 1
Crystallographic data for compounds **1** and **3–5**.

	1 0.25CHCl$_3$	**3**	**[4a·4b].H$_2$O**	**5**
Empirical formula	$C_{14}H_{22}N_3O_3P.0.25(CHCl_3)$	$C_{28}H_{48}Cl_3LaN_6O_8P_2$	$C_{58}H_{95}La_2N_{19}O_{32}P_4$	$C_{30}H_{52}LaN_9O_{13}P_2$
Formula weight	341.16	903.92	1972.23	947.66
T (K)	293(2)	100(2)	100(2)	293(2)
λ (Å)	0.71073	0.71073	0.71073	0.71073
Crystal system	monoclinic	orthorhombic	triclinic	monoclinic
Space group	*P21/c*	*Fdd2*	$P\bar{1}$	*P21/c*
a (Å)	9.6943(19)	14.4045(18)	10.8328(9)	12.066(6)
b (Å)	10.339(2)	39.958(3)	16.3636(14)	24.273(12)
c (Å)	19.501(4)	12.9802(9)	23.5928(19	15.530(6)
α (°)	90	90	99.816(2)	90
β (°)	104.05(3)	90	100.440(2)	101.53(3)
γ (°)	90	90	94.052(2)	90
V (Å^3)	1896.1(7)	7471.2(12)	4030.4(6)	4457(4)
Z	4	8	2	4
Calculated density (g cm^{-3})	1.195	1.607	1.625	1.412
Absorption coefficient (mm^{-1})	0.264	1.497	1.220	1.095
F(0 0 0)	722	3680	2012	1944
Crystal size (mm)	0.30 × 0.20 × 0.10	0.30 × 0.25 × 0.20	0.150 × 0.080 × 0.020	0.35 × 0.25 × 0.04
θ range for data collection (°)	2.17–25.97	2.04–27.98	1.27–28.00	1.58–26.97
Limiting indices	$0 \leqslant h \leqslant 11$ $0 \leqslant k \leqslant 12$ $-24 \leqslant l \leqslant 23$	$-18 \leqslant h \leqslant 18$ $-45 \leqslant k \leqslant 52$ $-12 \leqslant l \leqslant 17$	$-14 \leqslant h \leqslant 14$ $-21 \leqslant k \leqslant 21$ $-24 \leqslant l \leqslant 31$	$0 \leqslant h \leqslant 15$ $0 \leqslant k \leqslant 30$ $-19 \leqslant l \leqslant 19$
Reflections collected	3825	9929	33627	9420
Independent reflection	3609[R(int) = 0.0701]	3746[R(int) = 0.0290]	19260[R(int) = 0.0768]	9042[R(int) = 0.0882]
Refinement method	full-matrix least-squares on F^2	full-matrix least-squares on F^2	full-matrix least-squares on F^2	full-matrix least-squares on F^2
Completeness to theta (%)	97.5	99.8	99.0	93.1
Data/restraints/parameters	3609/9/225	3746/1/218	19260/0/947	9042/0/496
Goodness-of-fit (GOF) on F^2	1.021	1.000	1.008	1.089
Final R indices	R_1 = 0.0711, wR_2 = 0.1479	R_1 = 0.0204, wR_2 = 0.0418	R_1 = 0.0795, wR_2 = 0.1738	R_1 = 0.0863, wR_2 = 0.1691
R indices (all data)	R_1 = 0.1490, wR_2 = 0.1724	R_1 = 0.0221, wR_2 = 0.0424	R_1 = 0.1423, wR_2 = 0.2018	R_1 = 0.2048, wR_2 = 0.2072
Largest difference in peak and hole (e Å^{-3})	0.727 and −0.356	0.478 and −0.481	2.617 and −1.304	1.778 and −1.582

Ar–H), 7.23 (t, $^3J_{HH}$ = 7.6 Hz, 2H, Ar–H) ppm. $^{13}C\{^1H\}$ NMR (DMSO-d_6, 125.76 MHz, 298 K): δ = 44.57 (s, CH_2), 66.63 (d, $^3J_{PC}$ = 5.5 Hz, CH_2), 117.90 (d, $^3J_{PC}$ = 6.4 Hz, C_{ortho}), 121.48 (s), 128.79 (s), 139.82 (s) ppm. $^{31}P\{^1H\}$ NMR (DMSO-d_6, 202.46 MHz, 298 K): δ = 10.34 (s) ppm. IR (KBr, cm^{-1}): 3420, 3198, 2895, 1592, 1488, 1438, 1289, 1253, 1192, 1127, 1087, 1020, 963, 930, 748, 689, 500.

2.4. Preparation of ligand P(O)(PhC(O)NH)(NH(tert-C_4H_9))$_2$; (**2**)

N-Benzoyl, *N′*,*N″*-bis(*tert*-butyl) phosphoric triamide (**2**) was prepared similar to the reported procedure [37,38] and recrystallized in CH_3OH:CH_3CN (1:3). Yield 80%. Decom. point. 98 °C, *Anal.* Calc. for $C_{15}H_{26}N_3O_2P$: C, 57.86; H, 8.42; N, 13.50. Found: C, 57.72; H, 8.51; N, 13.41%. ^1H NMR (DMSO-d_6, 500.13 MHz, 298 K): δ = 1.21 (s, 9H, *tert*-Bu), 1.24 (s, 9H, *t*Bu), 4.00 (d, $^2J_{PH}$ =6.6 Hz, 2H, NH), 7.43 (t, $^3J_{HH}$ = 7.6 Hz, 1H, Ar–H), 7.62 (t, $^3J_{HH}$ = 7.3 Hz, 1H, Ar–H), 7.95 (m, 3H, Ar–H), 9.46 (b, 1H, NH) ppm. $^{13}C\{^1H\}$ NMR (DMSO-d_6, 125.76 MHz, 298 K): δ = 27.11 (s), 31.23 (d, $^3J_{PC}$ = 4.9 Hz), 50.35 (s), 50.92 (s), 127.97 (s), 128.21 (s), 131.82 (s), 168.19 (s, C=O) ppm. $^{31}P\{^1H\}$ NMR (DMSO-d_6, 202.46 MHz, 298 K): δ = 4.10 (s) ppm. IR (KBr, cm^{-1}): 3115, 2940, 1634, 1496, 1418, 1387, 1279, 1234, 1009, 957, 534.

2.5. General procedure for the preparation of complexes

To a stirred solution of $LaCl_3{\cdot}7H_2O$ or $La(NO_3)_3{\cdot}6H_2O$ (1 mmol) in 10 ml of acetonitrile was added a solution of corresponding ligands (2 mmol in 30 ml acetonitrile) at 60 °C. After 3 days stirring at room temperature, the resulting white solid was filtered. Crystals suitable for X-ray diffraction were obtained from CH_3OH/CH_3CN solutions of **3**, **4** and **5**.

2.6. Data for La(**1**)$_2$Cl$_3$(H$_2$O)$_2$; (**3**)

Yield 65%, M.p. 192 °C, *Anal.* Calc. for $C_{28}H_{48}Cl_3LaN_6O_8P_2$: C, 37.21; H, 5.35; N, 9.30. Found: C, 37.05; H, 5.43; N, 9.39%. ^1H NMR (DMSO-d_6, 500.13 MHz, 298 K): δ = 3.12 (m, 16H, CH_2), 3.44 (m, 16H, CH_2), 6.79 (m, $^3J_{HH}$ = 7.7 Hz, $^6J_{PH}$ = 1.0 Hz, 2H, Ar–H), 7.16 (m, 8H, Ar–H), 7.43 (d, $^2J_{PH}$ = 9.7 Hz, 2H, NH) ppm. $^{13}C\{^1H\}$ NMR (DMSO-d_6, 125.76 MHz, 298 K): δ = 44.34 (s), 66.43 (d, $^3J_{PC}$ = 5.9 Hz), 117.79 (d, $^3J_{PC}$ = 6.6 Hz), 120.05 (s), 128.56 (s), 142.35 (s) ppm. $^{31}P\{^1H\}$ NMR (DMSO-d_6, 202.46 MHz, 298 K): δ = 11.60 (s) ppm. IR (KBr, cm^{-1}): 3375, 3220, 2835, 1611, 1480, 1353, 1257, 1228, 1151, 1102, 1019, 967, 936, 834, 753, 686, 565, 502.

2.7. Data for [La(**1**)$_2$(NO$_3$)$_3$H$_2$O.La(**1**)$_2$(NO$_3$)$_3$CH$_3$CN].H$_2$O; (**4a.4b.H$_2$O**)

Yield 55%. M.p. 165 °C, *Anal.* Calc. for $C_{58}H_{95}La_2N_{19}O_{32}P_4$: C, 35.32; H, 4.85; N, 13.50. Found: C, 35.49; H, 4.91; N, 13.66%. ^1H NMR (DMSO-d_6, 500.13 MHz, 298 K): δ = 2.05 (s, 3H, CH_3), 3.01 (m, 32H, CH_2), 3.45 (m, 32H, CH_2), 5.01 (b, H_2O), 6.81 (m, $^3J_{HH}$ = 6.8 Hz, 4H), 7.15 (m, 16H), 7.20 (d, $^2J_{PH}$ = 9.8 Hz, 4H, NH) ppm. $^{13}C\{^1H\}$ NMR (DMSO-d_6, 125.76 MHz, 298 K): δ = 43.31 (s), 65.36 (d, $^3J_{PC}$ = 5.8 Hz), 116.74 (d, $^3J_{PC}$ = 6.9 Hz), 119.09 (s), 127.56 (s), 141.17 (s) ppm. $^{31}P\{^1H\}$ NMR (DMSO-d_6, 202.46 MHz, 298 K): δ = 11.59 (s) ppm. IR (KBr, cm^{-1}): 3360, 3300, 2845, 1593, 1485, 1441, 1381, 1296, 1259, 1131, 1109, 1021, 967, 943, 749, 690, 498.

2.8. Data for La(**2**)$_2$(NO$_3$)$_3$; (**5**)

Yield 68%. M.p. 265 °C, *Anal.* Calc. for $C_{30}H_{52}LaN_9O_{13}P_2$: C, 38.02; H, 5.53; N, 13.30. Found: C, 38.19; H, 5.61; N, 13.22%. ^1H NMR (DMSO-d_6, 500.13 MHz, 298 K): δ = 1.32 (s, 36 H, 4 *t*Bu), 7.48 (t, $^3J_{HH}$ = 7.8 Hz, 2 H), 7.59 (t, $^3J_{HH}$ = 7.4 Hz, 4 H), 7.89 (d, $^3J_{HH}$ = 7.3 Hz, 4 H) ppm. $^{13}C\{^1H\}$ NMR (DMSO-d_6, 125.76 MHz, 298 K): δ = 29.84 (d, $^3J_{PC}$ = 5.0 Hz, CH_3), 50.70 (s), 127.26 (s), 127.86 (s), 132.11 (s) ppm. $^{31}P\{^1H\}$ NMR (DMSO-d_6, 202.46 MHz, 298 K): δ = 3.82 (s) ppm. IR (KBr, cm^{-1}): 3305, 2965, 1617, 1566, 1453, 1386, 1330, 1279, 1225, 1180, 1152, 1020, 925, 892, 833, 788, 664, 561.

3. Results and discussion

3.1. Spectroscopic investigations

Some structural and electronic perturbations are occurred in the ligand structure upon complexation, due to the polarization effects and electron donation to the cation. The ^{31}P NMR resonances of **3** and **4** are shifted downfield with respect to the free ligand **1** (Table 2). This is consistent with an increase of partial positive charge on phosphorus atom. In ^1H NMR, a doublet at 5.11 ppm ($^2J_{PH}$ = 8.1 Hz) corresponds to the amine (aniline) proton in free ligand **1**. This signal shifts to 7.43 and 7.20 ppm in complexes **3** ($^2J_{PH}$ = 9.7 Hz) and **4** ($^2J_{PH}$ = 9.8 Hz), respectively. The $^2J_{PH}$ coupling constants increase comparatively from the free ligand **1** to complexes **3** and **4**, which is in line with the shortening of the P–N bonds. In free ligand **1**, ^1H NMR revealed a triplet signal at 6.98 ppm ($^3J_{HH}$ = 7.6 Hz) for the *para*-position hydrogen atom of aniline ring, that changes to a triplet of doublet signal at 6.79 ppm ($^3J_{HH}$ = 7.7 Hz, $^6J_{PH}$ = 1.0 Hz) in complex **3**. The $^3J_{PH}$ coupling constants are 2.0 and 4.3 Hz for hydrogen atoms in morpholine ring of complexes **3** and **4**, respectively. It should be noted that the phosphorus-hydrogen spin coupling depends on the distance and dihedral angle between two coupled atoms [39]. Herein, the suitable distance and dihedral angle between phosphorus and hydrogen atoms cause $^6J_{PH}$ and $^3J_{PH}$ coupling constants in complexes **3** and **4**, which are not appeared in free ligand **1**.

Crystallization of compound **2** in various solvents leads to different results. The NMR spectra and X-ray crystallography have corroborated that the crystallization of this compound in a mixture of $CHCl_3$ and *n*-C_7H_{16} produces two conformers in solution and solid state [38]. Herein, only one conformer of ligand **2** obtained by using the solvents with higher polarity (i.e., CH_3OH/CH_3CN), that is confirmed by the appearance of one signal at 4.10 ppm in $^{31}P\{^1H\}$ NMR spectrum. But, this conformer contains two unequal *tert*-butyl groups. ^1H NMR reveals two separated signal (1.21 and 1.24 ppm) for two *tert*-butyl groups. ^{13}C NMR spectrum indicates two different signals for *tert*-carbon atoms (50.92 and 50.35 ppm) and two signals for the methyl carbon atoms (singlet at 27.11 and doublet, $^3J_{PC}$ = 4.9 Hz, at 31.23 ppm) in **2**. These indicate that the two *tert*-butyl moieties have different orientation and

Table 2
Spectroscopic data of compounds **1**–**5**.

Compound	δ (^{31}P)(ppm)	$^2J_{PH}$ (Hz)	($^{2,3}J_{PC}$)$_{aliphatic}$ (Hz)	$^{3,6}J_{PH}$ (Hz)	$\nu_{P=O}$ (cm^{-1})	$\nu_{C=O}$ (cm^{-1})	ν_{N-H} (cm^{-1})
1	10.34	8.1	0.0, 5.5	0.0, 0.0	1192		3198
2	4.10	6.6	0.0, 4.9		1234	1634	3115
3	11.60	9.7	0.0, 5.9	2.0, 1.0	1151		3220
4	11.59	9.8	0.0, 5.8	4.3, 0.0	1131		3300
5	3.82		0.0, 5.0		1225	1617	3305

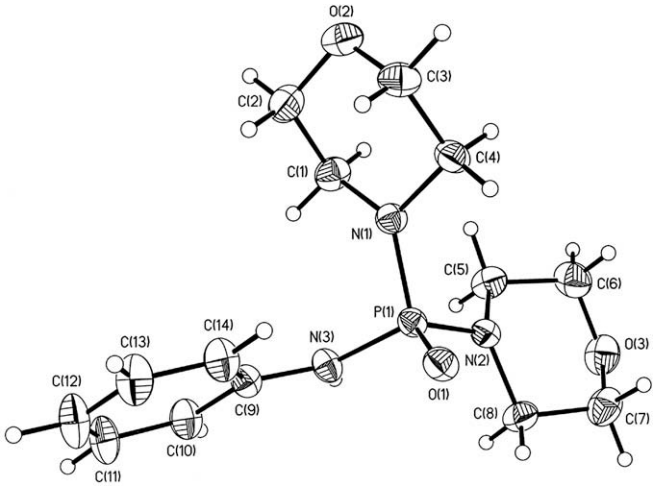

Fig. 1. Thermal ellipsoid plot of **1**. Ellipsoids are shown at 50% probability.

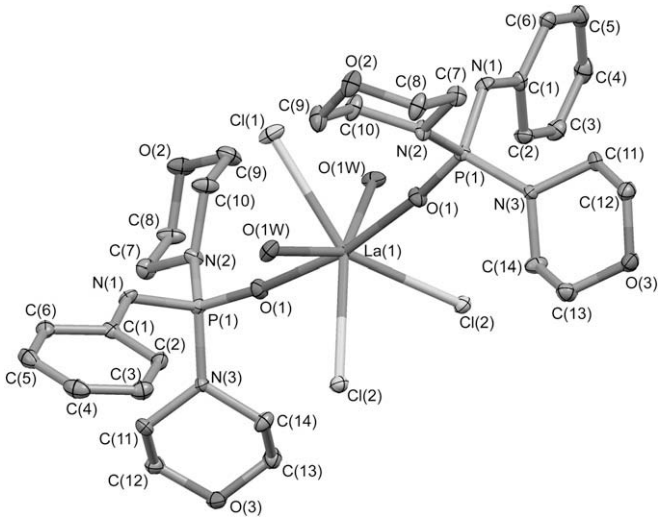

Fig. 2. ORTEP diagram (at the 50% probability level) of **3**, with the H atoms omitted for clarity.

they are not equivalent. The ^{1}H and ^{13}C NMR spectra of **5** indicate that the non equivalency of two *tert*-butyl moieties has been removed after complexation. The ^{1}H NMR spectrum of complex **5** shows one singlet peak at 1.32 ppm for *tert*-butyl protons. Corresponding ^{13}C NMR spectrum indicates one signal at 50.70 ppm for the *tert*-carbon atoms and a doublet at 29.84 ppm ($^{3}J_{PC}$ = 5.0 Hz) for the methyl carbon atoms.

A significant decreasing of the $\nu_{P=O}$ is observed by complexation of these phosphoryl containing ligands with metal ions. The IR spectra show that the P=O stretching frequency shifts considerably from 1192 cm^{-1} (in free ligand **1**) to 1151 and 1131 cm^{-1} in complexes **3** and **4**, respectively. But these shifts are relatively smaller in complex **5** in which the $\nu_{P=O}$ and $\nu_{C=O}$ are decreased about 9 and 17 cm^{-1} when compared with free ligand **2**. The large shifts in the position of P=O stretching frequency from the free ligand **1** to complexes **3** and **4**, confirm that the La–O_P interaction in **3** and **4** is stronger than that in **5**. This may be attributed to the weak M–L interaction in high coordinated complex **5**.

The direct relationship is observed between the N–H stretching frequency (ν_{N-H}) and $^{2}J_{PH}$ coupling constant in the order of **2** < **1** < **3** < **4** (see Table 2). It seems that the P–N bond strengthening affects the N–H vibrational frequency. It should be noted that the hydrogen bond gives rise to increase the X–H bond length (red shift) in X–H···Y system. This interaction leads to increase the X–H band intensity [40]. Here, the N–H band appears at 3198 cm^{-1} (sharp) in free ligand **1** and at 3220 cm^{-1} (medium) in complex **3**. As a result, the N–H band shifts toward higher frequencies by weakening of the hydrogen bond from N–H···O_P in **1** to N–H···Cl in **3**. The wide bands at 3375 and 3360 cm^{-1} in complexes **3** and **4** may be related to the O–H stretching frequencies.

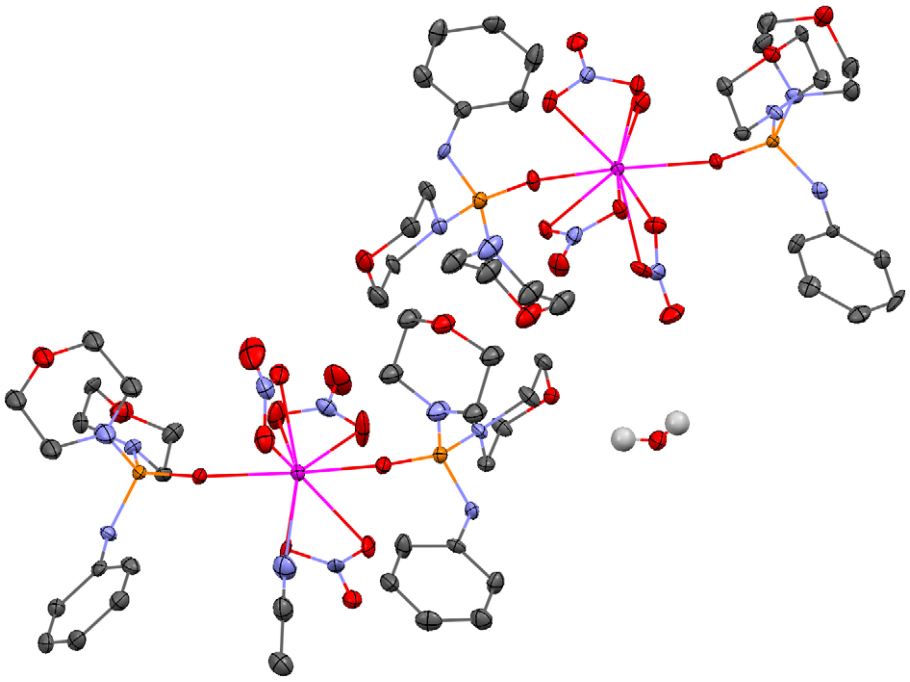

Fig. 3. Representation of three molecules **4a**, **4b** and H_2O in unit cell of compound **4**. The hydrogen atoms are shown only for H_2O.

3.2. Structural studies using X-ray crystallography

3.2.1. Structural comparison between the free ligands and coordinated ones

The molecular structure of compounds **1**, **3**, **4** and **5** are shown in Figs. 1–5 and selected structural parameters are given in Supplementary materials (Table S1). Upon complexation, the P=O bond length of free ligand **1** increases from 1.473(3) Å to 1.493(17 Å in **3**, 1.497(6) Å in **4a** and 1.492(7) Å in **4b**. Whereas, the mean P–N bond lengths decreases for example from P1–N3 = 1.649(3) Å in free ligand **1** to 1.642(2) Å for P1–N1 in **3** and to 1.635(8) Å for P2–N9 in **4a**. These observations represent the increasing of the P–N bond order. Lengthening of the P=O bond may be attributed to the polarization of phosphoryl group in the electrostatic field of metal cation, which has been suggested by Berny et al. [26]. Similarly, it can be considered that the partial charges on the phosphorus and nitrogen atoms increase because of the P=O bond polarization by metal ion (Scheme 3). Thus, the electrostatic interaction increases between phosphorus and nitrogen atoms. This polar bond overlaps with P–N σ bond [41], which may explain the shortening of the P–N bond in complex.

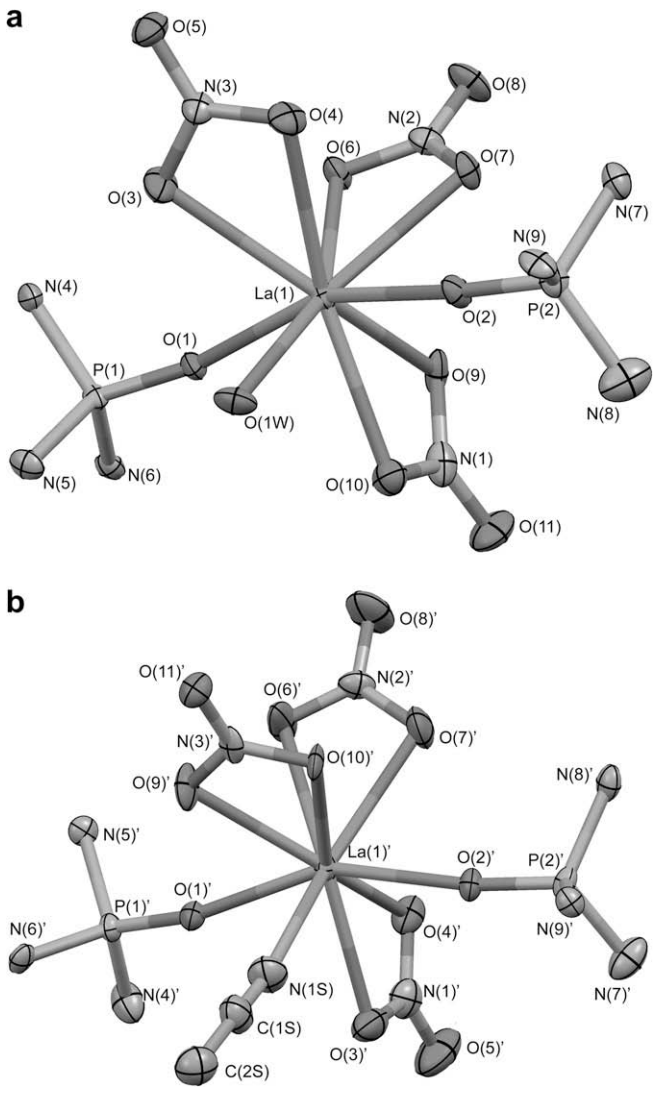

Fig. 4. Coordination structure in a) **4a** and b) **4b**. All hydrogen atoms were omitted for clarity and the amine groups reduced to their N atoms. Thermal ellipsoids are drawn at the 50% probability level.

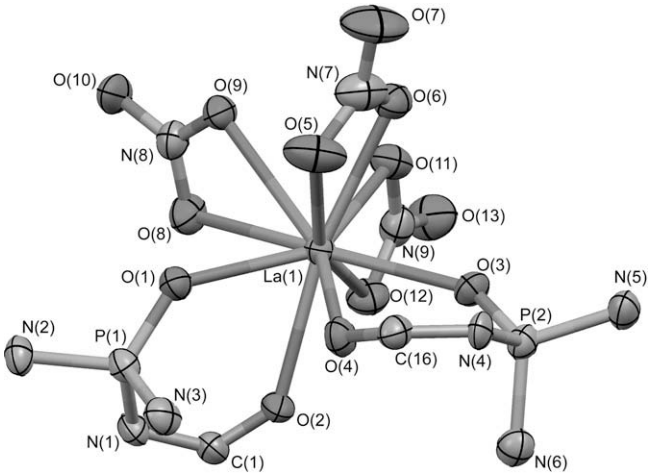

Fig. 5. View of the structure of **5**. Ellipsoids are shown at the 50% probability level. Hydrogen atoms are omitted for clarity and amine groups reduced to their N atoms.

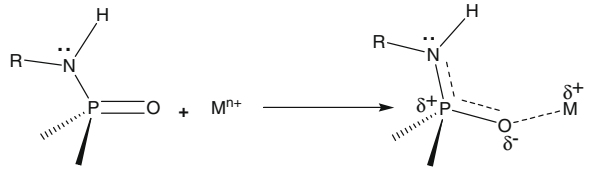

Scheme 3. Schematic representation of electronic reorganization in coordinated ligand.

The C=O and P=O groups adopt *anti* configuration as a result of the dipole–dipole repulsion. For instance, the O–P–N–$C_{carbonyl}$ torsion angles are −174.8(2)° and −176.6(2)° for two conformers in **2** [38]. These torsion angles vary to 44.1(10)° and 49.1(9)° for two coordinated ligands in **5**. The phosphoryl and carbonyl functional groups with torsion angles (O2–C1···P1–O1) and (O4–C16···P2–O3) take the nearly *syn* configuration in complex **5**. These changes are needed to bis-chelation of free ligand **2**.

The unit cell of complex **4** includes three independent molecules **4a**, **4b** and a free water molecule (Figs. 3 and 4). Moreover, one water molecule (*O*-donor) and acetonitrile (*N*-donor) are coordinated to the metal cation in **4a** and **4b**, respectively. This causes a difference in the La–O_P distances in **4a** and **4b**. For instance, the La1–O1 and La1–O2 are 2.427(6) Å in molecule **4a** that differ from La1′–O1′ (2.399(6) Å) and La1′–O2′ (2.417(6) Å) in molecule **4b**. Whereas, the O_N atoms are negatively charged in nitrate counter ion, the La···$O_{Nitrate}$ interaction is expected to be stronger than La···O_P in **4a** and **4b**. But the mean La–$O_{Nitrate}$ distances is longer than the La–O_P one in **4a** and **4b** (Table 3), probably due to the steric hindrance which is created by bis-chelation of the nitrate counter ion in the first shell of La^{3+}.

3.2.2. Comparison between the coordination ability of the P=O and C=O functional groups

The monodentate ligand **1** is coordinated to the La^{3+} cation as an *O*-donor in structures **3** and **4**, while ligand **2** (*O*,*O*′-donor) chelates the metal cation via P=O and C=O groups in structure **5**. Whereas, the phosphoryl group is more polarizable than the carbonyl group, the increasing of negative charge on the O_P atom is approximately two times more than that of O_C in complexation ($\Delta\delta^-(O_C < \Delta\delta^-(O_P)$ when $\Delta\delta^- = \delta^-(O)_{complex} - \delta^-(O)_{free\ ligand}$)[31]. In the bis-chelated complex **5**, the La–O_P distances of 2.438(7) and 2.427(7) Å are relatively shorter than the La–O_C distances

(2.553(7) and 2.587(7) Å). Therefore, it can be concluded that the La^{3+} ion interacts more strongly with the P=O functional group than the C=O counterpart.

3.2.3. The effect of monodentate and bidentate counter ions on the La–O_P distance

The quantum mechanical studies on $(R_3P{=}O)_n{\cdots}Ln(X)_3$ complexes (X= Cl^- and NO_3^-, n = 1, 2) have corroborated that the Ln–O_P distance increases from the chloride to the nitrate complexes due to the increased steric crowding around the cation with the bidentate counter ions [31]. Herein, the La–O_P distance of 2.397(2) Å in chloride complex (**3**) increases to 2.399(6), 2.417(6), 2.427(6) and 2.427(6) Å (for La1–O1, La1–O2, La1′-O1′ and La1′–O2′, respectively) in nitrate complex (**4**). In the gas phase, the P=O bond in chloride complex is expected to be longer than that in nitrate complex as a function of M–O_P bond strength [31]. However, in the solid state, it was found that the P=O bond in chloride complex is shorter than that in nitrate one, considering the P=O band in IR spectra (1151 *vs.* 1131 cm^{-1}). The theoretical (gas phase) and experimental (solid phase) results may differ, since the geometry of molecule may be influenced by packing and crystal field in the solid state. Unlike the gas phase, hydrogen bonds are formed in the solid phase. The nitrate counter ions are more involved in hydrogen bonds with respect to the chloride counter ions (see Section 3.2.4). This leads to remain a higher positive charge on La^{3+} cation due to a decreased electron density transfer from the nitrate to the La^{3+} cation. Consequently, the P=O bond may be more polarized and attenuated in nitrate complex.

3.2.4. Hydrogen bonding

The data of hydrogen bonds are represented in Supplementary materials, Table S2. Co-crystallization of solvent ($CHCl_3$) molecule was occurred in the structure of free ligand **1** via O(1)···Cl(2) electrostatic interaction. The hydrogen bond of N–H···O_P type is another feature in structure **1**. The hydrogen bond in the X–H···Y system is followed by electron density transfer from Y to the σ^*(X–H) antibonding orbital, which results in weakening of the X–H bond and red shift of the X–H vibrational frequency [34]. Similarly, it can be said that the σ^*(O–H) orbital is a better electron acceptor than the σ^*(N–H) orbital leading to the stronger O_W–H···O_M (O_M stands for $O_{Morpholine}$) hydrogen bond than the N–H···Cl in complex **3**. Moreover, the hydrogen bonds of type N–H···O_P ($d_{N\cdots O}$ = 2.938(5) Å and ∠N–H–O = 169°) in crystal lattice of free ligand **1** are replaced by weak N–H···Cl hydrogen bond ($d_{N\cdots Cl}$ = 3.388(2) Å and ∠N–H–Cl = 150°) in complex **3**, which is in agreement with increasing of the N–H stretching frequency from **1** to **3** in IR spectra. Another feature in complex **3** is the difference between La···Cl(1) and La···Cl(2) distances, $d_{La-Cl(1} < d_{La-Cl(2)}$. This seems to be related to the sharing of Cl(1) and Cl(2) ions in different C–H···Cl(1) and N–H···Cl(2) hydrogen bonds. Furthermore, the O_W–H···O_M hydrogen bonds between the hydrogen atoms of coordinated water molecules and oxygen of morpholine ring have formed in the complex **3**. These hydrogen bonds create a three-dimensional (3D) network which seems as butterfly-arrays along the *a*-axis of unit cell in complex **3** (Fig. 6). Various hydrogen bonds of O_W–H···O_W, O_W–H···O_M and N–H···O_N types make 3D framework in the crystal lattice of complex **4**. Comparison between the donor-acceptor distances in the complexes **3** and **4** shows that the nitrate counter ions are more contributed in hydrogen bonding than chloride counter ions (Table S2). This may have some effects on the M-L interaction as a result of decreasing electron density transfer from nitrate group to the La^{3+} cation.

Table 3
The mean values of La–O distance (d; Å) for compounds **3**–**5**.

Parameters	Compound			
	3	**4a**	**4b**	**5**
d(La–$O_{Phosphoryl}$)	2.397	2.427	2.409	2.432
d(La–$O_{Carbonyl}$)				2.570
d(La–$O_{Nitrate}$)		2.592	2.603	2.651
d(La–O_{Water})	2.516	2.513		

4. Conclusions

The monodentate *O*-donor P(O)(PhNH)$(NC_4H_8O)_2$ and bidentate *O*,*O*′-donor P(O)(PhC(O)NH)(NH(*tert*-C_4H_9))$_2$ were prepared and used to synthesis high-coordinated lanthanum(III) chloride and nitrate complexes. It is found that the polarity of solvent influences the crystalline sample. Coordination of the ligand is followed by a number of structural perturbations such as the changes in the bond lengths and bond angles, which are confirmed by spectroscopic evidences. The $^2J_{PH}$, $^3J_{PH}$ and $^6J_{PH}$ coupling constants increased significantly upon complexation. X-ray crystallography confirmed that the La^{3+} ion interacts more strongly with phosphoryl group than carbonyl counterpart. The experimental observations in the solid phase were fairly in good agreement with the gas phase data in the literature for all cases studied here, except for polarization of P=O in nitrate and chloride complexes. Unlike the gas phase, the P=O bond becomes more polarized in the nitrate

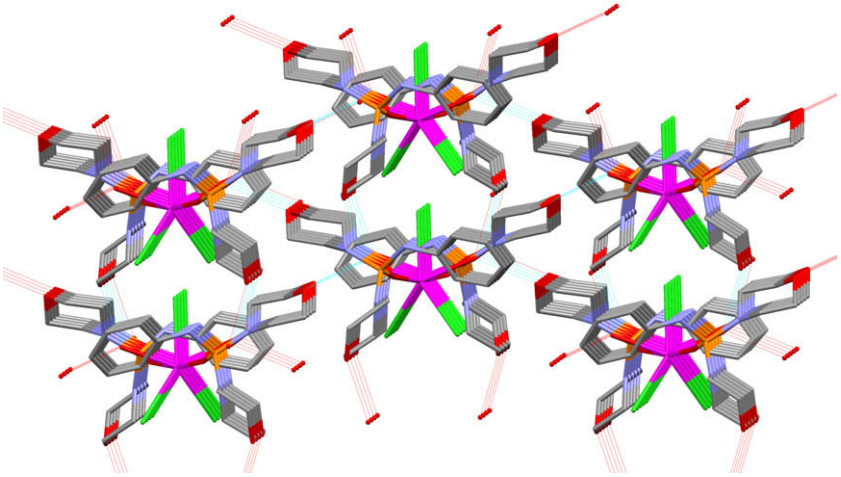

Fig. 6. The 3-D view along the *a*-axis produced by O_W–H···$O_{morpholine}$ hydrogen bonds in **3** (the hydrogen atoms are omitted for clarity).

complex than the same bond in chloride complex in the solid phase.

Acknowledgment

Support of this work by Tarbiat Modares University is gratefully acknowledged.

Appendix A. Supplementary material

CCDC 286213, 647432, 678072 and 265236 contain the supplementary crystallographic data for this paper. These data can be obtained free of charge from The Cambridge Crystallographic Data Centre via www.ccdc.cam.ac.uk/data_request/cif. Supplementary data associated with this article can be found, in the online version, at doi:10.1016/j.ica.2010.03.064.

References

[1] J.R. Morrow, L.A. Buttrey, V.M. Shelton, K.A. Berback, J. Am. Chem. Soc. 114 (1992) 1903.
[2] K. Wang, R. Li, Y. Cheng, B. Zhu, Coord. Chem. Rev. 190 (1999) 297.
[3] F.H. Li, G.H. Zhao, H.X. Wu, H. Lin, X.X. Wu, S.R. Zhu, H.K. Lin, J. Inorg. Biochem. 100 (2006) 36.
[4] G. Zhao, F. Li, H. Lin, H. Lin, Bioorg. Med. Chem. 15 (2007) 533.
[5] G.F. de Sa, O.L. Malta, C. de Mello Donega, A.M. Simas, R.L. Longo, P.A. Santa-Cruz, E.F. da Silva Jr, Coord. Chem. Rev. 196 (2000) 165.
[6] X.P. Yang, B.S. Kang, W.K. Wong, C.Y. Su, H.Q. Liu, Inorg. Chem. 42 (2003) 169.
[7] K. Kuriki, Y. Koike, Y. Okamoto, Chem. Rev. 102 (2002) 2347.
[8] A.L. Jenkins, O.M. Uy, G.M. Murray, Anal. Chem. 71 (1999) 373.
[9] K.L. Nash, Solvent Extr. Ion Exch. 11 (1993) 729.
[10] A. Bhattacharyya, P.K. Mohapatra, V.K. Manchanda, Solvent Extr. Ion Exch. 25 (2007) 27.
[11] M.R. Yaftian, M. Burgard, D. Matt, C.B. Dieleman, F. Rastegar, Solvent Extr. Ion Exch. 15 (1997) 975.
[12] L. Atamas, O. Klimchuk, V. Rudzevich, V. Pirozhenko, V. Kalchenko, I. Smirnov, V. Babain, T. Efremova, A. Varnek, G. Wipff, F. Arnaud-Neu, M. Roch, M. Saadioui, V. Bohmer, J. Supramol. Chem. 2 (2002) 421.
[13] G. Modolo, S. Nabet, Solvent Extr. Ion Exch. 23 (2005) 359.
[14] S. Barboso, A.G. Carrera, S.E. Matthews, F. Arnaud-Neu, V. Bohmer, J.F. Dozol, H. Rouquette, M.J. Schwing-Weill, J. Chem. Soc., Perkin Trans. 2 (1999) 719.
[15] E.P. Horwitz, A.C. Muscatello, D.G. Kalina, L. Kaplan, Sep. Sci. Technol. 16 (1981) 417.
[16] F. Arnaud-Neu, J.K. Browne, D. Byrne, D.J. Marrs, M.A. McKervey, P.O. Hagan, M.J. Schwing-Weill, A. Walker, Chem. Eur. J. 5 (1999) 175.
[17] Q.H. Jin, L. Ricard, F. Nief, Polyhedron 24 (2005) 549.
[18] M. Bosson, W. Levason, T. Patel, M.C. Popham, M. Webster, Polyhedron 20 (2001) 2055.
[19] L.J. Caudle, E.N. Duesler, R.T. Paine, Inorg. Chem. 24 (1985) 4441.
[20] Q.L. Guo, D.Q. Yuan, S.L. Ma, Y.C. Liu, W.X. Zhu, J. Mol. Struct. 752 (2005) 78.
[21] J. Fawcett, A.W.G. Platt, S. Vickers, M.D. Ward, Polyhedron 23 (2004) 2561.
[22] A.M.J. Lees, A.W.G. Platt, Inorg. Chem. 42 (2003) 4673.
[23] G. Oczko, J. Legendziewicz, V. Trush, V. Amirkhanov, New J. Chem. 27 (2003) 948.
[24] M. Borzechowska, V. Trush, I. Turowska-Tyrk, W. Amirkhanov, J. Legendziewicz, J. Alloys Compd. 341 (2002) 98.
[25] K.E. Gubina, J.A. Shatrava, V.A. Ovchynnikov, V.M. Amirkhanov, Polyhedron 19 (2000) 2203.
[26] F. Berny, N. Muzet, L. Troxler, A. Dedieu, G. Wipff, Inorg. Chem. 38 (1999) 1244.
[27] M. Baaden, F. Berny, C. Boehme, N. Muzet, R. Schurhammer, G. Wipff, J. Alloys Compd. 303 (2000) 104.
[28] L. Troxler, A. Dedieu, F. Hutschka, G. Wipff, J. Mol. Struct. (THEOCHEM) 431 (1998) 151.
[29] L. Troxler, M. Baaden, V. Bohmer, G. Wipff, J. Supramol. Chem. 12 (2000) 27.
[30] B. Coupez, C. Boehme, G. Wipff, Phys. Chem. Chem. Phys. 4 (2002) 5716.
[31] C. Boehme, G. Wipff, Inorg. Chem. 41 (2002) 727.
[32] C. Boehme, G. Wipff, Inorg. Chem. 38 (1999) 5734.
[33] K. Gholivand, H.R. Mahzouni, M.D. Esrafili, Theor. Chem. Acc. 2010, doi:10.1007/s00214-010-0743-5.
[34] A.Y. Li, J. Phys. Chem. A 110 (2006) 10805.
[35] H. Ghalla, N. Rekik, M. Baazaoui, B. Oujia, M.J. Wojcik, J. Mol. Struct. (THEOCHEM) 855 (2008) 102.
[36] G.M. Sheldrick, SHELXTL Programs, Version 5.1, Bruker AXS, Madison, WI, 1998.
[37] A.V. Kirsanov, R. Makitra, J. Gen. Chem. 26 (1956) 905.
[38] K. Gholivand, M. Pourayoubi, Z. Anorg. Allg. Chem. 630 (2004) 1330.
[39] J.G. Verkade, L.K. Quin, Phosphorus-31 NMR Spectroscopy, Stereochemical Analysis, VCH Publisher, 1987. pp. 365–385.
[40] A. Beyer, Th.R. Dyke, A. Karpfen, C. Sandorfy, P. Schuster, Topics in Current Chemistry, vol. 120, Springer-Verlag, Berline Heidelberg, 1984. pp. 1–40.
[41] K. Gholivand, M. Pourayoubi, Z. Shariatinia, H. Mostaanzadeh, Polyhedron 24 (2005) 655.